Slow evolution of elliptical galaxies induced by dynamical friction

III. Role of density concentration and pressure anisotropy

S. E. Arena and G. Bertin

Università degli Studi di Milano, Dipartimento di Fisica, via Celoria 16, 20133 Milano, Italy
e-mail: [Serena.Arena;Giuseppe.Bertin]@unimi.it

ABSTRACT

Context. Dynamical friction is expected to play an important role in a variety of astrophysical contexts, yet we still lack a quantitative understanding of this basic mechanism and of its effects. In fact, numerical simulations have shown that in inhomogeneous systems the classical idealized description, given by Chandrasekhar (1943), may have severe limitations, possibly related to the global nature of the processes that are involved.

Aims. In this paper we address two issues. Firstly, we study how dynamical friction depends on the density concentration and on the pressure anisotropy of the host galaxy. For the purpose, we consider models characterized by a "realistic" distribution function and compare the behavior of dynamical friction in these systems to that found in other simpler models (often used in the past because of their mathematical convenience). Secondly, we study the response of the galaxy to the infall, by dynamical friction, of heavy objects ("satellites") taken in a variety of initial configurations.

Methods. The investigation is carried out by using a numerical laboratory set up in previous papers of this series. The process of dynamical friction is studied in terms of its strength (i.e., its efficiency to drag a satellite toward the galaxy center) and in terms of its ability to circularize the orbit of the satellite under friction. The response of the galaxy is studied in terms of the induced modifications to the galaxy density distribution and shape and of the changes produced to its phase space properties.

Results. (1) We find that, within the range of our models, the pressure anisotropy present in the host galaxy has little effect on dynamical friction. Instead, the shape of the galaxy density profile is very important. The classical idealized description, although with an effectively smaller Coulomb logarithm, appears to be applicable to galaxy models characterized by a broad core (such as a polytrope) but not to concentrated models. Correspondingly, in contrast to the behavior found in models with a broad core, the orbits of satellites captured in concentrated models are not circularized by dynamical friction. To a large extent, these results confirm trends already known in the literature; in this respect, we also confirm the value of some simple modifications to the classical formulae proposed in the literature. (2) The induced evolution in the host galaxy reflects the initial conditions adopted for the captured satellite. Satellites spiraling in on quasi-circular orbits tend to modify the pressure tensor of the host galaxy in the tangential direction, while satellites captured along quasi-radial orbits tend to induce pressure anisotropy in the radial direction. While satellites captured along quasi-circular orbits make a galaxy change its shape from spherical to oblate, satellites captured along quasi-radial orbits tend to induce a shape in the host galaxy of the prolate type. This result suggests that the shape of early-type galaxies may just result from the characteristics of occasional mergers rather than being directly related to the effectiveness of the radial-orbit instability during the process of formation via collisionless collapse, as often argued in the past.

Key words. methods: N-body simulations – galaxies: elliptical and lenticular, cD – galaxies: evolution –
galaxies: kinematics and dynamics

1. Introduction

Elliptical galaxies are essentially collisionless stellar systems. If they were purely collisionless isolated stellar systems, they might in principle remain in a dynamical equilibrium configuration for all their life. In practice, some evolution is expected to take place. In this series of papers (see Bertin et al. 2003, hereafter Paper I; and Arena et al. 2006, hereafter Paper II) we have investigated a process of dynamical evolution that should be ubiquitous. This is the evolution induced in the galaxy by the interaction with satellites or a population of heavy objects (such as a system of globular clusters or clumps of dark matter), which are dragged in toward the galaxy center by dynamical friction.

The classical formula of dynamical friction was derived under highly idealised conditions (Chandrasekhar 1943). In contrast, real systems are inhomogeneous and generally characterized by a non-Maxwellian distribution function; in addition, satellites or other heavy objects dragged in by dynamical friction are captured on complex orbits, on which resonant effects are expected. Therefore, in the last two decades one line of research has tried to determine, by means of semi-analytical tools or dedicated numerical simulations, to what extent the classical formula of dynamical friction is applicable to more complex and realistic situations.

Theoretically, dynamical friction results from resonant effects and is often interpreted in terms of interaction with a "wake" induced in the otherwise collisionless stellar system by the passage of the heavy object under investigation (e.g., see Mulder 1983; Tremaine & Weinberg 1984; Palmer & Papaloizou 1985; Weinberg 1986, 1989; see also Sect. 2 of Paper I). An interesting connection has been drawn with the general statement of the fluctuation-dissipation theorem (Kandrup 1983; Nelson & Tremaine 1999). Additional references on the subject have been recorded in Papers I and II.

With the help of self-consistent numerical simulations (see Bontekoe & van Albada 1987, hereafter BvA87, and Bontekoe 1988, hereafter B88), it became clear that the process of dynamical friction depends on the model of the galaxy where it takes place. In particular, it was found that for a satellite dragged toward the center in a polytropic galaxy model (BvA87, confirmed in Paper I), the classical formula is basically applicable, although with a value of the Coulomb logarithm smaller than unity, and the orbits of satellites are circularized by dynamical friction; it was also noted that in these broad-core models dynamical friction seems to disappear when the satellite reaches the central regions. In turn, in galaxies described by a King model (B88, Hashimoto et al. 2003) the classical formula fails (because one finds an effective Coulomb logarithm that varies with radius) and orbits are not circularized.

It has been suggested that, if the maximum impact parameter $b_{\max}$ appearing in the definition of the Coulomb logarithm were chosen properly, a description in terms of the classical formula of dynamical friction might remain applicable. One choice (Hashimoto et al. 2003; Spinnato et al. 2003) has been $b_{\max} = r_s$, where r_s is the distance of the satellite from the center of the galaxy. Another proposed choice (Just & Peñarrubia 2005) has been $b_{\max} \sim \rho/|\nabla\rho|$, so that the maximum impact parameter should be identified with the local scale of the density gradient. In practice, it is likely that the process of dynamical friction in inhomogeneous systems reflects some *global* effects that cannot be captured by variations on the classical formula. Therefore, it is important to widen the set of models on which the process of dynamical friction is studied by means of numerical simulations in order to see whether some general trends can be identified for the behavior of such a complex phenomenon.

In general, past theoretical investigations have referred to objects moving through stellar systems characterized by an isotropic (quasi-)Maxwellian distribution function. In some cases (e.g., see van den Bosch et al. 1999; Jiang & Binney 2000; Spinnato et al. 2003; and Just & Peñarrubia 2005), simulations are carried out on models constructed numerically by imposing a desired density profile and an assumed Maxwellian velocity distribution, evolved for a few dynamical times to reach approximate equilibrium. One notable exception, also because of its interest in the evolution of the host system, is a study of the process of dynamical friction on galaxies inside clusters (Binney 1977), considered as non-spherical systems supported by an anisotropic velocity distribution.

Recently, a few papers have addressed the important issue of the orbital decay of objects treated as "live" stellar systems (Peñarrubia et al. 2004; Fujii et al. 2005), with the possibility that the captured object is eventually disrupted by tidal interactions inside the host galaxy. These investigations certainly go in the direction of a more realistic study of the relevant astrophysical issues; yet, the complications and the number of parameters introduced make it even harder to extract from them a general statement on the ways dynamical friction proceeds.

Most of these investigations have focused on the fate of the heavy object under friction, while in the present series of papers (see Papers I and II) we have discussed the mechanism of dynamical friction in the more general context of the evolution of the stellar system where the processes occur. Recently, some cosmological issues have made this point of view even more important. In fact, it has been noted that evolution induced by dynamical friction (in contrast to the expectations from a scenario of adiabatic evolution; see Paper II) tend to lead to systems with softer density profiles (El-Zant et al. 2001; Paper I; El-Zant et al. 2004; Ma & Boylan-Kolchin 2004;

Nipoti et al. 2004), with a significant impact on the current debate about the observational counterparts to the universal halo density profiles found in cosmological simulations (Navarro et al. 1996; Moore et al. 1998; Ghigna et al. 2000; Navarro et al. 2004). This line of work has motivated the formulation of cosmological simulations based on the use of the Fokker-Planck approach (Ma & Bertschinger 2004; see also Evans & Collett 1997; Weinberg 2001), for which it would be crucial to know whether dynamical friction can be, at least approximately, described in terms of local diffusion coefficients.

In this paper we study the dependence of the process of dynamical friction (and of the response of the host galaxy) on the density and pressure anisotropy profile of the stellar system where dynamical friction takes place. The study thus goes in the direction of investigating the slow evolution of more realistic models of elliptical galaxies and is intended to broaden the set of systems in which the process of dynamical friction, which is likely to have a global character, is studied quantitatively. To do so, we consider a family of stellar dynamical models, called $f^{(\nu)}$ models, that has been widely studied, especially in relation to its ability to describe the products of collisionless collapse (Stiavelli & Bertin 1987; Bertin & Trenti 2003; Trenti & Bertin 2005; Trenti et al. 2005). This is basically a one-parameter family of models, with significant variations of density and pressure anisotropy profiles (from the concentrated models that reproduce the observed $R^{1/4}$ law to models with a broader core that are close to being unstable against the radial-orbit instability). Along this family of models, density concentration and pressure anisotropy change in a way determined by the physically justified distribution function. Therefore, in order to decouple the role of density concentration from that of pressure anisotropy, in this paper we also consider two series of models for which pressure anisotropy is specified and varied independently, by following the so-called Osipkov-Merritt prescription (Osipkov 1979; Merritt 1985): a Plummer model, as a prototypical broad core model, and a Jaffe (1983) model, as a prototypical concentrated model. For this study, we consider single satellites starting from a variety of initial conditions, and, following the arguments of Papers I and II, shells of satellites that allow us to study the relevant mechanisms within a quasi-spherical environment.

In Sect. 2 we present the models and the code. In Sect. 3 we define the adopted units and the relevant diagnostics and we present some test simulations. In Sect. 4 we describe the results of the simulations for the process of dynamical friction in $f^{(\nu)}$ models compared with those observed in Plummer and Jaffe models with varying anisotropy. In Sect. 5 we give the results relative to the induced evolution in the previously considered galaxy models. In Sect. 6 we provide a general discussion and draw the main conclusions.

2. The models and the code

2.1. The host galaxy

The basic models used in the numerical simulations to represent the initial state of the host stellar system are constructed from three different distribution functions.

The first is the $f^{(\nu)}$ distribution function:

$$f^{(\nu)} = A e^{-[aE + d(J^2/|E|^{3/2})^{\nu/2}]}, \tag{1}$$

for $E < 0$ and zero otherwise. The related models, constructed by imposing the self-consistent Poisson equation, have been briefly considered in Paper II and have been extensively described in a separate article (Trenti & Bertin 2005). Here, we

recall that E and J are the single-star energy and angular momentum and that the four real constants A, a, d, and ν are positive. A model is thus specified by two dimensional scales and two dimensionless parameters, such as ν and the dimensionless central potential $\Psi = -a\Phi(0)$. In the following, we take $\nu = 3/4$ (the properties of the models would have only a mild dependence on ν) and thus refer to a one-parameter family of models. All the models are characterized by a quasi-isotropic central region and by radial pressure anisotropy in their outer parts. For higher values of Ψ the models are more concentrated and more isotropic, with properties similar to those of some observed ellipticals (in particular, they are characterized by an $R^{1/4}$ projected density profile) and of the products of collisionless collapse obtained in a variety of numerical experiments; for lower values of Ψ the models develop a relatively broad core and become more anisotropic, so that for $\Psi < 4$ they are unstable with respect to the radial-orbit instability (see Trenti & Bertin 2005; and Trenti et al. 2005). In the following study, we would like to investigate the process of dynamical friction not only under "realistic" density profiles (higher values of Ψ), but also close to conditions of marginal stability of the host system ($\Psi \approx 4$).

The simulations that we will describe in Sect. 4 cover the range of $f^{(\nu)}$ models with Ψ running from 4.0 to 6.6. These models have different density and anisotropy profiles. As mentioned above, as Ψ increases, the models are more concentrated and less anisotropic. However, given the finite size of the satellite and the fact that the change of the density profile with Ψ mostly affects the innermost region (see Trenti & Bertin 2005), all these models will appear to have similar density concentration (which is higher than that characteristic of the polytropic model studied in Papers I and II or that of the Plummer models) comparable to the density concentration of the Jaffe models (see below for further description). Therefore, simulations on models with varying Ψ will mostly test the behavior of dynamical friction while the pressure anisotropy of the host galaxy is varied.

To study cases in which the pressure anisotropy profile can be varied independently of the density profile, we have then considered the following two distributions functions.

One is the f_P distribution function (Merritt 1985):

$$f_P = A(-aQ)^{7/2}\left[1 - \frac{b^2}{r_\alpha^2} + \frac{63}{144}\frac{b^2}{r_\alpha^2}\frac{1}{(aQ)^2}\right] \qquad (2)$$

for $-1/a \leq Q \leq 0$ and zero otherwise. The quantities E and J are here combined in $Q = E + J^2/(2r_\alpha^2)$. This distribution function generates a Plummer density profile:

$$\rho(r) = \frac{3M}{4\pi}\frac{b^2}{(b^2 + r^2)^{5/2}}, \qquad (3)$$

and an Osipkov–Merritt pressure anisotropy profile:

$$\alpha(r) \equiv 2 - \frac{\langle v_\theta^2\rangle + \langle v_\phi^2\rangle}{\langle v_r^2\rangle} = \frac{2r^2}{r^2 + r_\alpha^2}, \qquad (4)$$

where r_α is the anisotropy radius defined as the radius where $\alpha(r_\alpha) = 1$. The constant a is related to the gravitational constant G and the mass of the galaxy M by $a = b/(GM)$ and A and b are two dimensional scales. The half-mass radius r_M is related to b by $b = \sqrt{2^{2/3} - 1}\,r_M$. With these models we will investigate the role of pressure anisotropy at fixed density profile, for the case of a broad-core distribution.

The other distribution function (see Binney & Tremaine 1987, Eq. (4-143), p. 241) generates a Jaffe (1983) density profile:

$$\rho(r) = \frac{M}{4\pi}\frac{b}{r^2(b + r)^2} \qquad (5)$$

and the above-described Osipkov-Merritt anisotropy profile. For this model $b = r_M$. With these models we will investigate the role of pressure anisotropy at fixed density profile, for the case of a concentrated distribution. Given the singularity present in the density distribution at $r = 0$, in our finite-resolution simulations the creation of an initial configuration according to the last model requires that we let evolve the initial configuration briefly, so that it settles into a quasi-equilibrium state close to the singular analytic model.

2.2. Single satellites and shells of satellites

We will study the orbital decay of single satellites and, as we did in Papers I and II, of satellites distributed within a quasi-spherical shell.

Each satellite is described by a rigid Plummer sphere, characterized by mass and radial scale M_s and R_s (i.e., we take $M = M_s$ and $b = R_s$ in Eq. (3)), respectively; we consider scales M_f and R_f when we refer to one element of a shell made of N_f fragments (in general we consider $M_f = M_s/N_f$).

We take single satellites moving initially on circular, quasi-circular, eccentric, and quasi-radial orbits. We discriminate among different levels of eccentricity of the initial orbit by referring to the quantity v_{0s}/v_c, where v_{0s} is the magnitude of the initial velocity of the satellite and v_c is the velocity of the satellite that would correspond to a circular orbit at the chosen initial radius in the given galaxy potential; in any case, the velocity vector of the satellite at the beginning of the simulation has no radial component.

We then consider two different configurations for "shells of fragments", both extensively described in Papers I and II. The first configuration is defined by the following shell density profile:

$$\rho_{\text{shell}}(r) = \rho_0\exp\left[-4(r - r_{\text{shell}}(0))^2/R_{\text{shell}}^2\right], \qquad (6)$$

for $|r - r_{\text{shell}}(0)| \leq R_{\text{shell}}$ and vanishing otherwise. Here $r_{\text{shell}}(0)$ is the initial position of the shell where the density is ρ_0 and R_{shell} is the shell half-thickness. In the presence of this shell density distribution, it is necessary to recalculate the initial galaxy model as described in Sect. 3.2.2. of Paper I. The shell density profile is then sampled with N_f simulation particles (the "fragments") with mass $M_f = M_{\text{shell}}/N_f$, where M_{shell} is the total mass of the shell, initially placed on circular orbits.

The second configuration is constructed by extracting the fragments directly from the distribution function of the galaxy following the distribution of (eccentric) orbits characteristic of the assumed distribution function (see Sect. 3.2.3 of Paper I).

2.3. The code

The galaxy evolution is computed with the same collisionless (mean field) particle-mesh code described in Paper II; for details, see Trenti et al. (2005) and Trenti (2005). For the purpose of the present study, the choice of the code and the general set-up of the simulations are justified in Papers I and II. The galaxy distribution function is sampled with N particles by means of a Monte Carlo procedure. The same method is used to derive the

position of the N_f fragments of the shell, for runs that involve the study of shells of satellites. Each simulation particle of the galaxy is subject to the mean field produced by the entire galaxy and to the direct action of the satellites present. Each satellite interacts directly with all the other satellites (when more than one satellite is present) and all the simulation particles representing the galaxy.

3. Units, diagnostics, and test simulations

3.1. Units

The adopted units are 10 kpc for length, 10^{11} $M_\odot$ for mass, and 10^8 yr for time. Thus, velocities are measured in units of 97.8 km s^{-1} and the value of the gravitational constant G is ≈ 4.497. We refer to models for which the total mass is $M = 2 \times 10^{11}$ $M_\odot$ and the half-mass radius is $r_M = 3$ kpc. Correspondingly, the dynamical time $t_d = GM^{5/2}/(2K)^{3/2}$ (here K is the total kinetic energy of the galaxy) falls in the range $0.18-0.25 \times 10^8$ yr.

3.2. Diagnostics

The strength of dynamical friction is studied in terms of the effective Coulomb logarithm $\ln \Lambda$, as done in Paper I and in BvA87, and directly in terms of the friction coefficient γ, defined by the relation $\boldsymbol{a}_{df} = -\gamma \hat{\boldsymbol{v}}_s$, where $\boldsymbol{a}_{df}$ is the deceleration suffered by a satellite as a result of dynamical friction and $\hat{\boldsymbol{v}}_s$ is its velocity in the frame of reference locally comoving with the galaxy particles that are responsible for the dynamical friction process. We will compare the values of these two quantities, measured in the simulations, with those expected from the Chandrasekhar theory.

The detailed steps for the computation of $\ln \Lambda$ from the simulations were given in Sect. 5.1 of Paper I. In particular, we recall that, following BvA87, the quantity $\ln \Lambda$ is estimated from the relation $4\pi G^2 \ln \Lambda = -v_s(dE_{sat}/dt)/(M_s^2 \rho_G F(\hat{v}_s))$, where E_{sat} and M_s are the energy and the mass of the satellite, ρ_G represents the density of the galaxy, and $F(\hat{v}_s)$ is the fraction of particles with velocity, with respect to the local direction of the motion of the satellite, smaller than $\hat{v}_s$. The fraction F is computed on the basis of the actual distribution function, which is not assumed to be Maxwellian.

As to the friction coefficient γ, we may start from the basic equation for the rate of change of the satellite energy

$$\frac{dE_{sat}}{dt} = -\gamma M_s \boldsymbol{v}_s \cdot \hat{\boldsymbol{v}}_s \sim -\gamma M_s v_s^2. \tag{7}$$

Therefore, extracting the "experimental" value of γ from the simulations requires similar steps to those required for the extraction of $\ln \Lambda$ and is actually simpler, because no sampling of the galaxy velocity space is needed. The friction coefficient is a dimensional quantity and thus, from our simulations, $(1/\gamma)$ will come out expressed in units of 10^8 yr.

For a single satellite dragged in by dynamical friction on a quasi-circular orbit, when we will compare the above-defined measured values of $\ln \Lambda$ and γ to those expected from the Chandrasekhar theory, $\ln \Lambda_{Ch}$ and γ_{Ch}, for simplicity we will refer to the values of the Coulomb logarithm and of the friction coefficient computed from the classical theory on the basis of the properties of the *unperturbed* galaxy at each radius r; similarly, for the velocity of the satellite entering the relevant formulae, we will refer to the circular velocity, as a function of r,

expected in the adopted initial galaxy model from the relation $v_s(r) = \sqrt{r d\Phi_G/dr}$.

In the classical theory the value of the maximum impact parameter b_{max}, which appears in $\ln \Lambda_{Ch}$, has been subject to different interpretations; furthermore, such theory was developed for point-like masses. In this paper, for point-like satellites, we take $\ln \Lambda_{Ch} = \ln [3M/(2M_s)]$, which coincides with the formula given by Chandrasekhar if evaluated at $r = r_M$, with $b_{max} = 3r_M$. In turn, for extended objects, we refer to the formula suggested by White (1976), given that our satellites are characterized by a Plummer density profile:

$$\ln \Lambda_{Ch} = \frac{1}{2} \left[\ln \left(1 + \frac{b_{max}^2}{R_s^2} \right) - \frac{b_{max}^2}{b_{max}^2 + R_s^2} \right], \tag{8}$$

where we set $b_{max} = 3r_M$; for simplicity, we keep the notation $\ln \Lambda_{Ch}$, even though the latter formula was not provided by Chandrasekhar. (Note that the Coulomb logarithm for a point-like satellite depends on its mass, while for an extended object it depends on its radial size.) A satellite will be considered to be point-like when R_s is smaller than the radius where the two expressions of the Coulomb logarithm given above have the same value.

The discrepancy between the measured value and the expected value of the Coulomb logarithm will be often expressed in terms of the quantity $\lambda(r) \equiv \ln \Lambda / \ln \Lambda_{Ch}$. Note also that in the classical theory the Coulomb logarithm and the coefficient of dynamical friction are related to each other through Eq. (7).

As in Paper I, in our plots we will often use the dimensionless Lagrangian radial coordinate $M(r)/M$ (based on the adopted initial galaxy model) instead of the radial coordinate r, so as to compare directly our results with those of BvA87. This choice has the effect of expanding the linear radial scale in the inner region, especially for radii smaller than the half mass radius r_M.

A global measure of the strength of dynamical friction is given by the fall time t_{fall} of a satellite, or of a shell of satellites, relative to a given initial radius $r_s(t = 0) = r_0$, i.e., by the time taken to reach the center of the galaxy.

We will also study whether orbits tend to be circularized by dynamical friction. The amount of circularization is calculated by checking the evolution of the ratio R_{min}/R_{max} of the pericenter to the apocenter of the satellite along its orbit.

Finally, the effects of dynamical friction on the host galaxy are studied by following the evolution of several quantities: the galaxy density profile $\rho(r)$, the pressure anisotropy profile $\alpha(r)$, the mean velocity profile $\langle v \rangle(r)$ (as is known, during the fall of a single satellite the galaxy may acquire some net rotation), the central density softening $(\Delta \rho / \rho)_{r=0}$, the shape parameters ϵ and η, and the global anisotropy parameter $k \equiv 2K_r/K_T$, where K_r and K_T are the total kinetic energy of the galaxy in the radial and tangential directions respectively. The radial profiles are defined by averaging the relevant quantities inside spherical shells, given the fact that the galaxy remains quasi-spherical in the course of evolution. The definition of the pressure anisotropy profile $\alpha(r)$ extends that of Eq. (4) to the case when mean motions, possibly induced in the galaxy, are present. The slight departure from spherical symmetry is then quantified by the two shape parameters, defined as $\epsilon = b/a$ and $\eta = c/a$, where $a \geqslant b \geqslant c$ are the lengths of the axes of the inertia tensor (see Trenti et al. 2005; and Trenti 2005), so that $\epsilon = 1$ identifies the oblate case and $\eta = \epsilon$ the prolate case.

Table 1. Test runs.

Run	Galaxy model	r_α/r_M	k
T1	$f^{(\nu)}, \Psi = 4.0$	0.9	1.84
T2	$f^{(\nu)}, \Psi = 4.6$	1.1	1.70
T3	$f^{(\nu)}, \Psi = 5.0$	1.2	1.62
T4	$f^{(\nu)}, \Psi = 5.4$	1.3	1.57
T5	$f^{(\nu)}, \Psi = 6.6$	1.7	1.40
T6	Polytrope	∞	1.00
T7	Plummer	1000	1.00
T8	Plummer	5	1.06
T9	Plummer	1.4	1.43
T10	Jaffe	1000	1.00
T11	Jaffe	5	1.06
T12	Jaffe	1.4	1.32
T13	Jaffe	0.75	1.66

Table 2. Equilibrium of the host stellar system.

Run	$\Delta r/r|_1$	$\Delta r/r|_2$	$\Delta\epsilon/\epsilon$	$\Delta\eta/\eta$	$\Delta k/k$
T1	0.14	0.01	0.16	0.17	0.04
T2	0.08	0.01	0.06	0.06	0.02
T3	0.05	0.01	0.016	0.02	0.01
T4	0.05	0.01	0.01	0.02	0.01
T5	0.04	0.008	0.007	0.01	0.01
T6	0.04	0.007	0.005	0.005	0.01
T7	0.03	0.007	0.005	0.006	0.008
T8	0.04	0.009	0.006	0.008	0.007
T9	0.03	0.007	0.006	0.008	0.01
T10	0.03	0.01	0.006	0.007	0.02
T11	0.04	0.04	0.006	0.007	0.02
T12	0.04	0.05	0.007	0.008	0.02
T13	0.05	0.06	0.006	0.009	0.02

Table 3. Stability of the orbit of a test particle and global conservations.

Run	$\Delta r_s/r_s$	$\Delta E_{sat}/E_{sat}$	$\Delta E_{tot}/E_{tot}$	$\Delta J_{tot}/J_{tot}$
T1	0.05	0.02	1.1×10^{-5}	1.8×10^{-3}
T2	0.07	0.01	8.4×10^{-6}	9.7×10^{-5}
T3	0.05	0.01	5.5×10^{-6}	4.7×10^{-5}
T4	0.06	0.01	3.6×10^{-6}	5.3×10^{-6}
T5	0.06	0.01	5.4×10^{-6}	3.4×10^{-5}
T6	0.05	0.01	7.0×10^{-6}	4.3×10^{-5}
T7	0.05	0.01	4.1×10^{-6}	6.3×10^{-6}
T8	0.04	0.01	4.1×10^{-6}	1.2×10^{-5}
T9	0.05	0.01	3.3×10^{-6}	1.8×10^{-5}
T10	0.07	0.02	5.2×10^{-6}	2.0×10^{-5}
T11	0.08	0.03	5.2×10^{-6}	1.2×10^{-4}
T12	0.08	0.03	5.2×10^{-6}	2.1×10^{-5}
T13	0.09	0.03	5.3×10^{-6}	2.1×10^{-4}

3.3. Test simulations

In the following section, we will show the results from a large set of simulations covering a wide range of physical conditions. In all these simulations and in the test runs described in the present subsection, the galaxy is sampled by $N = 250\,000$ simulation particles. Several tests performed earlier, and discussed in Paper I (see Sect. 5.1) and in Paper II (see Sect. 4), have demonstrated the adequacy of this number of simulation particles for the goals that we have set.

Table 1 lists the properties of several test runs that have been performed to check the overall performance of the code in relation to the models considered in this paper. In these test runs, a single satellite of very small mass $M_s = 10^{-9} M$ is placed initially on a circular orbit at $r_0 = 3.3 r_M$, with circular velocity v_c (in physical units, this is in the range 260–300 km s^{-1}). The Table specifies the type of galaxy model that is used and the value of its total anisotropy parameter.

The simulations are carried out for 30 dynamical times. Table 2 summarizes some observed limits on the galaxy evolution. The second column lists the maximum variation $\Delta r/r|_1$ of the radii of the spheres containing from 1% to 5% of the total mass of the galaxy; the third column gives the maximum variation $\Delta r/r|_2$ of the radii of the spheres containing from 50% to 99% of the galaxy mass; the fourth and fifth columns list the relative variations of the shape parameters and the last column the variation in the total pressure anisotropy. The significant variations noted for run T1 reflect the fact that the equilibrium $f^{(\nu)}$ model with $\Psi = 4$ is close to the margin of the radial orbit instability (Polyachenko & Shukhman 1981; Trenti & Bertin 2005).

Table 3 summarizes the results of the test runs from the point of view of the stability of the satellite orbit and of the global conservations. The second column ($\Delta r_s/r_s$) and the third column ($\Delta E_{sat}/E_{sat}$) give the relative variations of the radial position and of the energy of the satellite; the last two columns represent the conservation of total energy and angular momentum per dynamical time for the entire system (galaxy plus satellite).

At our disposal we also have a test simulation to check the equilibrium of the galaxy in the presence of a shell of fragments, i.e. run $D3$ of Paper II (with $N_f = 25\,000$ fragments of radius $R_f = 0.33 r_M$ and mass $M_f = 8 \times 10^{-6} M$); the results are in agreement with those of the corresponding model in the absence of the shell described above.

4. Dynamical friction in models characterized by different concentrations and various amounts of pressure anisotropy

Table 4 lists the main characteristics of simulations of the fall of a single satellite in $f^{(\nu)}$ models, which are the main focus of interest of this paper. Similarly, Table 5 summarizes the properties of other simulations performed on different models (see Sect. 2.1), for which the amount of pressure anisotropy can be varied independently of the density profile; for these runs, $M_s/M = 0.1$ and $r_0/r_M = 3.3$. As indicated in the tables, we have considered different combinations of mass M_s, radius R_s, initial position r_0, and initial velocity v_{0s} of the satellite (relative to the galaxy mass M, half-mass radius r_M, and circular velocity v_c at r_0).

Table 6 lists the simulations for the case of shells of satellites (see Sect. 2.2) in $f^{(\nu)}$ models. Following the notation of Paper I, runs labeled by B refer to the first type of shell (with fragments on circular orbits) while runs labeled by BT refer to the second type of shell (with fragments on non-circular orbits extracted from the distribution function of the galaxy). The models labeled by Ψ for runs of type B are slightly different from the corresponding models used for simulations with a single satellite, because the equilibrium configuration has to be re-computed in the presence of the shell, as mentioned in Sect. 2.2. In all these runs the half-thickness of the shell is $R_{shell} = 0.33 r_M$.

Table 4. Runs with a single satellite in selected $f^{(v)}$ models.

Run	Ψ	M_s/M	R_s/r_M	r_0/r_M	v_{0s}/v_c	Purpose
F1	5.0	0.07	0.33	3.3	0.96	Varying
F2	5.0	0.10	0.33	3.3	0.96	M_s
F3	5.0	0.14	0.33	3.3	0.96	and
F4	5.0	0.07	0.03	3.3	0.96	R_s
F5	5.0	0.10	0.03	3.3	0.96	
F6	5.0	0.14	0.03	3.3	0.96	
F7	5.0	0.10	0.06	3.3	0.96	
F8	5.0	0.10	0.17	3.3	0.96	
F9	5.0	0.10	0.06	3.3	0.99	
F10	5.0	0.005	0.33	1.0	0.99	
F11	5.0	0.10	0.33	1.0	0.96	Varying
F12	5.0	0.10	0.33	2.0	0.96	r_0
F13	5.0	0.10	0.33	6.0	0.96	
F14	4.0	0.10	0.33	3.3	0.96	Varying Ψ
F15	4.6	0.10	0.33	3.3	0.96	(quasi
F16	5.4	0.10	0.33	3.3	0.96	circular
F17	6.6	0.10	0.33	3.3	0.96	orbit)
F18	5.0	0.10	0.33	3.3	0.99	
F19	5.0	0.10	0.33	3.3	0.40	
F20	4.0	0.10	0.33	3.3	0.50	Varying Ψ
F21	4.6	0.10	0.33	3.3	0.50	and R_s
F22	5.0	0.10	0.33	3.3	0.50	(moderately
F23	5.0	0.10	0.17	3.3	0.50	eccentric
F24	5.4	0.10	0.33	3.3	0.50	orbit)
F25	6.6	0.10	0.33	3.3	0.50	
F26	5.0	0.10	0.33	3.3	0.70	
F27	4.0	0.10	0.33	3.3	0.30	Varying Ψ
F28	5.0	0.10	0.33	3.3	0.30	(eccentric
F29	6.6	0.10	0.33	3.3	0.30	orbit)
F30	4.0	0.10	0.33	3.3	0.10	Varying Ψ
F31	5.0	0.10	0.33	3.3	0.10	(quasi-radial
F32	6.6	0.10	0.33	3.3	0.10	orbit)

Table 5. Runs with a single satellite in galaxy models with different combinations of density concentration and pressure anisotropy.

Run	Model	r_α/r_M	k	R_s/r_M	v_{0s}/v_c
PO1	Polytrope	∞	1	0.33	0.98
PO2	Polytrope	∞	1	0.33	0.1
PO3	Polytrope	∞	1	0.33	0.5
PO4	Polytrope	∞	1	0.33	0.7
PO5	Polytrope	∞	1	0.06	0.98
PL1	Plummer	1000	1	0.33	0.98
PL2	Plummer	1000	1	0.33	0.5
PL3	Plummer	5.0	1.06	0.33	0.98
PL4	Plummer	5.0	1.06	0.33	0.5
PL5	Plummer	5.0	1.06	0.33	0.7
PL6	Plummer	5.0	1.06	0.06	0.98
PL7	Plummer	1.4	1.43	0.33	0.98
PL8	Plummer	1.4	1.43	0.33	0.5
JA1	Jaffe	1000	1	0.33	0.98
JA2	Jaffe	1000	1	0.33	0.5
JA3	Jaffe	5.0	1.06	0.33	0.98
JA4	Jaffe	5.0	1.06	0.33	0.5
JA5	Jaffe	1.4	1.32	0.33	0.98
JA6	Jaffe	1.4	1.32	0.33	0.5
JA7	Jaffe	0.75	1.66	0.33	0.98
JA8	Jaffe	0.75	1.66	0.33	0.5
JA9	Jaffe	0.75	1.66	0.33	0.7
JA10	Jaffe	0.75	1.66	0.06	0.98

Table 6. Runs with a shell of N_f fragments ($R_{shell}/r_M = 0.333$).

Run	Ψ	N_f	M_{shell}/M	R_f/r_M	$r_{shell}(0)/r_M$	Purpose
B1	5.0	20	0.10	0.33	1.0	Varying
B2	5.0	100	0.10	0.33	1.0	N_f
B3	5.0	20	0.10	0.066	1.0	Varying
B4	5.0	20	0.10	0.033	1.0	R_f
B5	5.0	20	0.10	0.017	1.0	
B6	5.0	20	0.07	0.033	1.0	Varying
B7	5.0	20	0.14	0.333	1.0	R_f and
B8	5.0	20	0.14	0.033	1.0	M_{shell}
B9	4.0	20	0.10	0.033	1.0	Varying
B10	6.6	20	0.10	0.033	1.0	Ψ
B11	5.0	20	0.10	0.033	0.5	Varying
B12	5.0	20	0.10	0.033	2.0	$r_{shell}(0)$
BT1	5.0	20	0.10	0.33	1.0	Varying
BT2	4.0	20	0.10	0.33	1.0	Ψ

4.1. Local properties of dynamical friction

In this subsection we focus on the mechanism of dynamical friction, by measuring its local strength in the simulations by means of the coefficient of dynamical friction γ and of the Coulomb logarithm $\ln \Lambda$, as defined in Sect. 3.2. Some of the results, especially the measured behavior in relation to the density concentration of the host galaxy and a curious behavior noted with respect to the direction of motion of the satellite, will actually demonstrate that dynamical friction cannot be reduced to a purely local process as envisaged in the classical theory.

4.1.1. The coefficient of dynamical friction

In Fig. 1, the coefficient of dynamical friction measured in the simulations (left column) is compared to the expectations from the classical theory (right column), in a given $f^{(v)}$ model for the host galaxy with $\Psi = 5$. The top panels refer to an extended satellite (runs $F1-F3$) of varying mass. The middle panels describe the case of a point–like satellite (runs $F4-F6$). The bottom panels illustrate the case of a satellite with given mass, with varying radial size (runs $F2$, $F5$, $F7$, and $F8$). The observed profiles of $\gamma(r)$ are systematically less steep than the corresponding profiles $\gamma_{Ch}(r)$ expected from the classical theory and, in general, the observed dynamical friction is smaller than expected. On the other hand, the scaling of the coefficient of dynamical friction with satellite mass and radial size is in general agreement with that predicted by the classical theory. This confirms results already obtained in BvA87.

In addition, no significant variations in the coefficient $\gamma(r)$ are observed by changing the model of the galaxy in the range $\Psi = 4.0-6.6$. This suggests that the coefficient of dynamical friction depends only very weakly on the pressure anisotropy content of the galaxy model, at least within realistic situations (as described by the anisotropy profiles $\alpha(r)$ characteristic of the family of $f^{(v)}$ models).

We have also checked that a single satellite and a fragment of equal mass and radius extracted from the spherical shell of run $B1$ feel the same amount of friction, at least for the radial range where such a comparison has been made. We recall that the study of dynamical friction for a shell of fragments has the advantage of offering a better controlled symmetry, but may include additional collective effects related to satellite-satellite interactions.

By considering the process of dynamical friction on eccentric orbits (runs $F19-F32$) we have met a curious effect, illustrated in Fig. 2. Apparently, the dynamical friction felt when
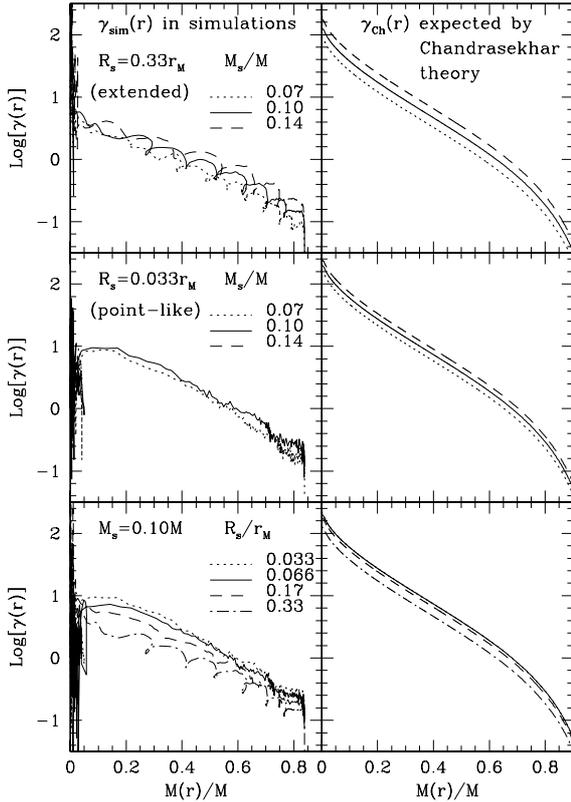
Fig. 1. The coefficient of dynamical friction in the $f^{(\nu)}$ galaxy model with $\Psi = 5$, for varying satellite mass and radial size. Observed coefficient of dynamical friction $\gamma(r)$ (*left panels*) measured in the simulations of the fall of a single satellite vs. expected coefficient $\gamma_{\mathrm{Ch}}(r)$ (*right panels*), as a function of the dimensionless Lagrangian radius $M(r)/M$. The observed coefficient in the simulations is generally smaller than expected, with differences that become more significant in the inner regions. With respect to the classical theory, a similar scaling with satellite mass and radial size is noted.

Fig. 2. Coefficient of dynamical friction measured on eccentric orbits. The *left panel* refers to measurements recorded at instants when the satellite is inbound (i.e., moving towards the center of the galaxy) while the *right panel* records measurements made when the satellite is outbound (moving away from the galaxy center). The dotted line refers to the fall of a satellite along a quasi-circular orbit (run $F18$), crosses and dots to eccentric orbits with initial velocity v_{0s}/v_c of 0.7 (run $F26$) and 0.5 (runs $F22$), respectively.
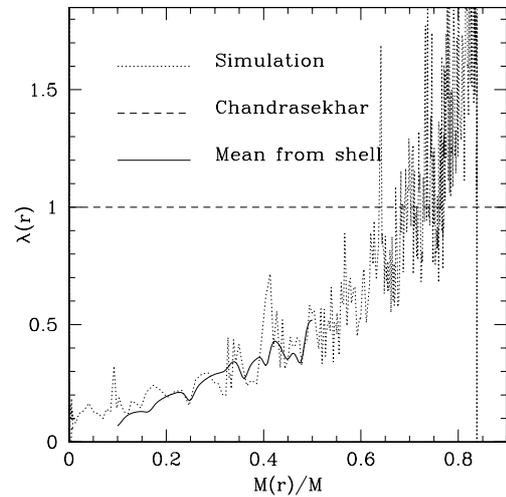
Fig. 3. Coulomb logarithm measured in the $f^{(\nu)}$ galaxy model with $\Psi = 5$. The dotted line represents $\lambda(r)$ measured in run $F18$, for a satellite initially placed on a circular orbit (a very similar behavior has been found in the corresponding runs for different $f^{(\nu)}$ models with varying Ψ). The dashed horizontal line indicates the expectations from the classical theory. The solid line shows the average value of $\lambda(r)$ found for the 20 fragments of simulation $B1$.

a satellite is "inbound", i.e. moving towards the center of the galaxy, is larger than the friction suffered when it is "outbound". In addition, the friction felt by the satellite when it falls towards the center increases with the eccentricity of the orbit. Therefore, dynamical friction appears to depend on the direction of the velocity vector of the satellite relative to the direction of the density gradient of the host galaxy.

4.1.2. The Coulomb logarithm

To compare the behavior observed in our simulations with other results reported in the literature, starting with BvA87, we have measured the strength of dynamical friction along the orbit of the satellite also in terms of the Coulomb logarithm. For $f^{(\nu)}$ galaxy models, the discrepancy between measured ($\ln \Lambda$) and predicted value ($\ln \Lambda_{\mathrm{Ch}}$) depends on the location where the measurement is made, in the sense that $\lambda \equiv \ln \Lambda / \ln \Lambda_{\mathrm{Ch}} = \lambda(r)$, as illustrated in Fig. 3.

Figure 4, as a counterpart to Fig. 2, illustrates the curious dependence, noted earlier in this section, of the friction strength on the direction of motion of the satellite for eccentric orbits.

4.1.3. Role of the density concentration and of the pressure anisotropy of the galaxy

We have performed a similar analysis of the coefficient of dynamical friction and of the Coulomb logarithm in other models, with the following results.

The shape of the density distribution plays an important role in determining the strength of dynamical friction. In models with a broad core, such as the polytropic and Plummer models of runs PO and PL, dynamical friction is weaker than expected but can be reconciled with the classical theory by rescaling the friction coefficient or the Coulomb logarithm by a constant factor (see left panels of Fig. 5). In turn, the study of the concentrated models (runs JA) confirms the discrepancies already noted in the $f^{(\nu)}$ models (see right panels of Fig. 5).

Different amounts of pressure anisotropy at fixed density profile have negligible effects on the strength of dynamical friction (see Fig. 5).
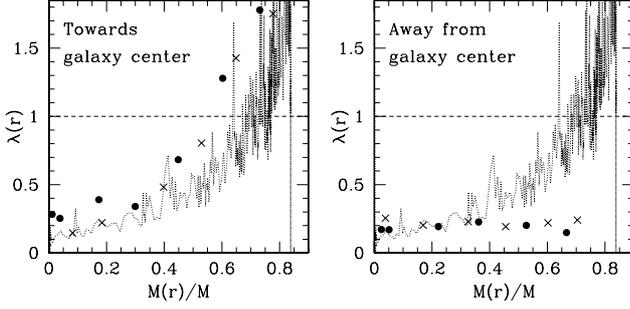
Fig. 4. Coulomb logarithm measured on eccentric orbits. Symbols and overall layout are as in Fig. 2. Note that outbound satellites appear to feel a friction strength consistent with a constant $\ln \Lambda$, while inbound satellites feel a friction strength consistent with that characteristic of quasi-circular orbits.
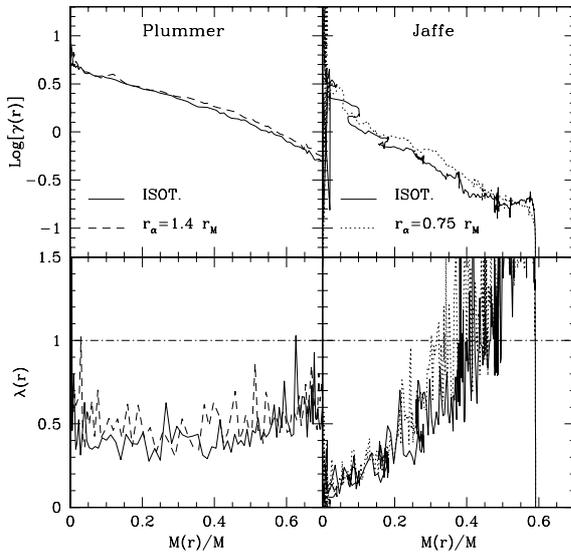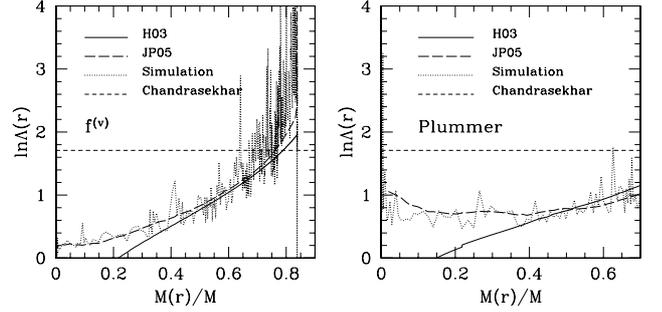

Fig. 6. Comparison between the Coulomb logarithm measured in our simulations and the prediction of two formulae suggested in the literature. The *left panel* refers to the $f^{(v)}$ galaxy model with $\Psi = 5$ and the *right panel* to the Plummer model. Solid lines and long dashed lines represent the prediction by Hashimoto et al. (2003) and by Just & Peñarrubia (2005), respectively. Dotted lines represent $\ln \Lambda(r)$ measured in runs $F18$ (*left*) and $PL1$ (*right*), for a satellite initially placed on a circular orbit. Short dashed horizontal lines indicate the expectations from the classical theory.

4.2. Global properties of dynamical friction

In this subsection we focus on the mechanism of dynamical friction, by measuring its global properties in terms of the fall time t_{fall} of a satellite, or of a shell of satellites, relative to a given initial radius $r_s(t = 0) = r_0$, and of the process of circularization of the satellite orbits.

4.2.1. The fall time

The fall time can be seen as the integral form of the coefficient of dynamical friction. Therefore, a consequence of the smaller values of γ observed in the simulations (see Sect. 4.1.1), with respect to the values predicted by the classical theory, is a greater fall time of the satellite. This is illustrated in the top panels of Fig. 7.

The top left panel of Fig. 7 represents the orbital decay of a single satellite initially placed on a circular orbit as observed in our simulations (run $F18$; solid line) compared to the expectations of the classical theory (dotted line); the observed fall time is about twice the expected value. The function $r_{\text{Ch}}(t)$ for the classical theory is computed using Eq. (7) with the classical expression for γ_{Ch}, under the assumption that locally the satellite moves on a circular orbit. Here the host galaxy is described by an $f^{(v)}$ model with $\Psi = 5$.

In the top right panel of Fig. 7, the solid line represents the observed orbital decay of one of the 20 fragments of a spherical shell for run $B1$, in the same galaxy model. The dashed line represents the case of a single satellite of equal mass ($M_s = 0.005M$) and radial size ($R_s = 0.33r_M$), for run $F10$. The dotted line gives the function $r_{\text{Ch}}(t)$ from the classical theory. Since the mass of the fragment ($B1$) or of the satellite ($F10$) is 20 times smaller than that of the satellite illustrated in the left panel ($F18$), the evolution observed is slower; note that a direct quantitative comparison between the two panels cannot be made easily, because the initial location of the satellite is different in the two cases. Surprisingly, the fall of the fragment in the shell is significantly slower than that of a single satellite of the same mass (run $F10$) falling alone inside the galaxy.

The bottom left panel of Fig. 7 represents the orbital decay of a single satellite (run $F22$) initially placed on an eccentric orbit ($v_{0s} = 0.5v_c$). The bottom right panel represents the fall of a shell (run $BT1$), extracted from the galaxy distribution function,
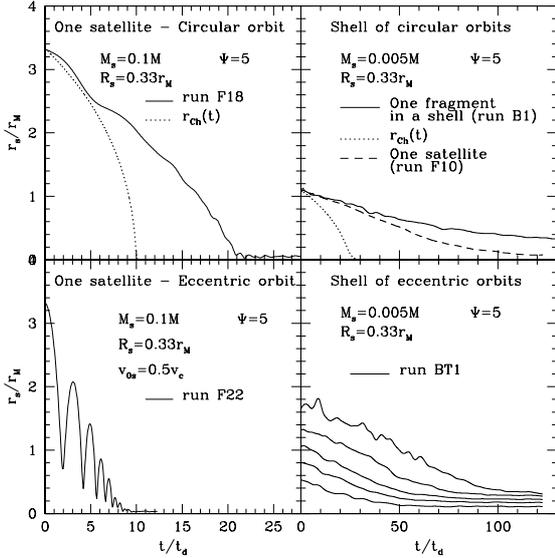

Fig. 5. Coefficient of dynamical friction (*top panels*) and Coulomb logarithm (*bottom panels*) for models with different degrees of density concentration and pressure anisotropy. *Left panels* refer to the broad core Plummer models, with different contents of pressure anisotropy: isotropic (run $PL1$, solid line) and radially anisotropic with $r_\alpha = 1.4r_M$ (run $PL7$, dashed line). *Right panels* refer to the concentrated Jaffe models: isotropic (run $JA1$, solid line) and radially anisotropic with $r_\alpha = 0.75r_M$, $k = 1.66$ (run $JA7$, dotted line). The effect of pressure anisotropy on the strength of dynamical friction is negligible, in contrast with that of density concentration.

4.1.4. Comparison with two modifications of the classical Coulomb logarithm proposed in the literature

In Fig. 6 we compare the value of the Coulomb logarithm measured in our simulations with the prediction of two simple modifications proposed by Hashimoto et al. (2003) and by Just & Peñarrubia (2005). Adapted to the case of our satellites characterized by a Plummer density profile, the two formulae are, respectively, $\ln \Lambda_{\text{H}} = \ln[r/(1.4R_s)]$ and $\ln \Lambda_{\text{JP}} = \ln[Q_0\rho(r)/(1.3R_s|\nabla\rho|)]$, where $Q_0 \approx 1$. For the two galaxy models considered in this comparison, good agreement with the second formula is found by setting $Q_0 = 2.72$, while the first formula appears to fail in the inner regions of the galaxy.

Fig. 7. Orbital decay produced by dynamical friction. *Top left*: fall of a single satellite (run *F*18, solid line) compared to the expectation from the classical theory (dotted line). *Top right*: fall of a fragment in a shell (run *B*1, solid line) and of a single satellite of same mass and radius (run *F*10, dashed line), compared to the expectation from the classical theory (dotted line). *Bottom left*: fall of a single satellite initially placed on an eccentric orbit (run *F*22). *Bottom right*: fall of a spherical shell of fragments (run *BT*1; the solid lines from the bottom represent the radii of the spheres containing 15, 35, 55, 75, and 95% of the mass of the shell).

Fig. 8. Dependence of the fall time on various properties of the satellite and of the galaxy. All panels display the fall time of a single satellite starting at $r_0 = 3r_M$. The *top two panels* represent the variation of $t_{\rm fall}$ on the satellite mass for an extended (*left panel*, runs *F*1, *F*2, and *F*3) and a point-like (*right panel*, runs *F*4, *F*5, and *F*6) satellite. The *middle left*, the *middle right*, and the *bottom left panels* show, respectively, the dependence of the fall time on the radial size of the satellite (runs *F*2, *F*5, *F*7, and *F*8), on the parameter Ψ characterizing the $f^{(\nu)}$ galaxy model (runs *F*2, *F*14, *F*15, *F*16, and *F*17), and on the eccentricity of the satellite orbit (runs *F*2, *F*18, *F*22, *F*26, *F*28, and *F*31). In the *top four panels*, filled circles refer to results from the simulations, triangles to the expectations from classical theory.

with fragments on a variety of eccentric orbits. The solid lines identify the radii of the spheres containing (from the bottom) 15, 35, 55, 75, and 95% of the mass of the fragments, respectively.

Figure 8 illustrates the dependence of the fall time on various properties of the satellite and of the host galaxy. The two top panels show the dependence on satellite mass for extended (left) and point-like (right) satellites. The middle left panel illustrates the dependence on the radial size of the satellite. The bottom panel shows the dependence on the eccentricity of the satellite orbit. As shown in the middle right panel, no significant differences are found by varying the value of Ψ of the $f^{(\nu)}$ model considered. In the top four panels, filled triangles refer to the expectations of the classical theory and dots to the values observed in the simulations.

In a series of polytropes with increasing size of the central core, B88 had noted that a single satellite is actually unable to reach the center in the course of its orbit. We found a similar behavior in simulations of models with a broad core (both in a polytropic model, *PO*5, and in a Plummer model, *PL*6). For single satellites in $f^{(\nu)}$ models this effect is not observed, probably because the size of the central core in these concentrated models is too small with respect to that of the satellite; on the other hand, in simulations of shells of fragments initially placed on circular orbits in concentrated $f^{(\nu)}$ models, the shell does not actually reach the center of the galaxy, but rather settles down into a quasi-equilibrium configuration of finite size (see bottom right panel of Fig. 7). Possibly, this latter behavior results from the fact that in the final stages the shell of fragments collectively mimicks the presence of a broad core.
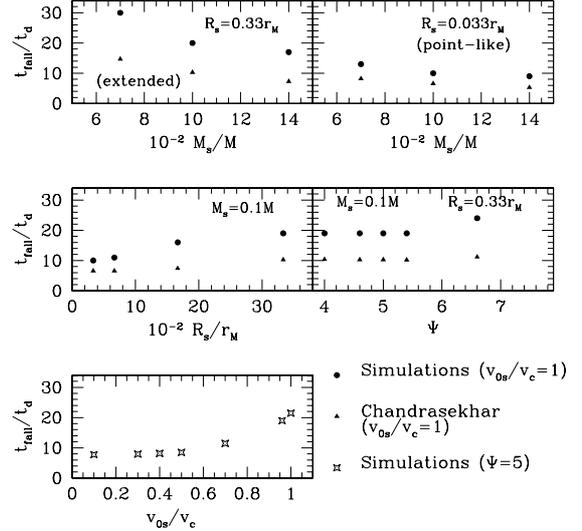
4.2.2. Circularization of orbits?

Dynamical friction may circularize initially eccentric orbits (see Tremaine et al. 1975). This effect has been observed in some simulations of broad core galaxies (e.g., in a polytrope, BvA87), but has been shown to be absent in the more concentrated King models (see B88). To contribute to the study of this problem, we have performed several numerical experiments in which the satellite starts from the outer regions of a galaxy described by a concentrated $f^{(\nu)}$ model, with a velocity vector in the tangential direction, but with speed smaller than that of the corresponding circular orbit at the same initial position. We have then followed the evolution of the ratio $R_{\rm min}/R_{\rm max}$, computed along the orbit covered by the satellite. This study shows that, in practice, within the family of $f^{(\nu)}$ models orbits are *not* circularized by dynamical friction.

One example is given in the top panel of Fig. 9, where the evolution of the ratio $R_{\rm min}/R_{\rm max}$ is shown for the orbit of the single satellite of run *F*22, starting with $v_{0s}/v_c = 0.5$ and falling in an $f^{(\nu)}$ model with $\Psi = 5$. The orbit initially increases and then slightly decreases its eccentricity, in practice with no evidence for circularization.

Changing the properties of the host galaxy within the family of $f^{(\nu)}$ models (runs *F*20, *F*21, *F*22, *F*24 and *F*25), at fixed initial eccentricity, does not lead to significant changes in the observed circularization. In turn, we note that, by starting from quasi-radial orbits, some circularization appears to take place (compare the result for run *F*31 with those for runs *F*2, *F*22, *F*26, and *F*28 in the middle panel of Fig. 9).

We have also looked for the process of circularization during the fall of a spherical shell made of $N_f = 20$ fragments on eccentric orbits (run *BT*1). The results are illustrated in the bottom panel of Fig. 9, which displays the distribution of the
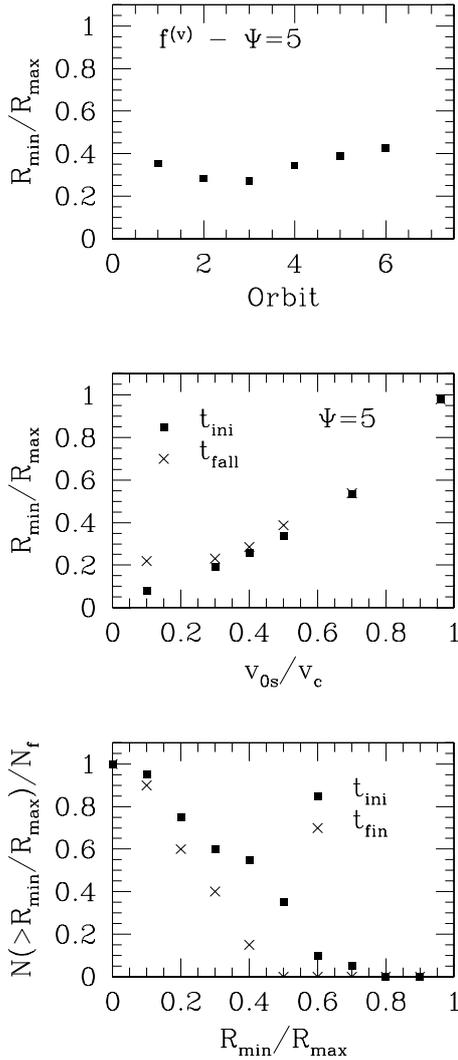
Fig. 10. Circularization of orbits in different galaxy models. Independently of pressure anisotropy, orbits are circularized in broad core models (runs *PL*2 and *PL*8) and remain eccentric in concentrated models (runs *JA*2 and *JA*6). The *x*-axis counts the number of turns made by the satellite starting from $t = 0$.

Fig. 9. Circularization of orbits in the $f^{(v)}$ model with $\Psi = 5$. *Top panel*: evolution of the orbit "aspect ratio" $R_{\min}/R_{\max}$ during the fall of a single satellite (run F22). The *x*-axis counts the number of turns made by the satellite starting from $t = 0$. *Middle panel*: initial (filled squares) and final (crosses) data points for the case of the fall of a single satellite on eccentric orbits (runs F2, F22, F26, F28, and F31). *Bottom panel*: initial (filled squares) and final (crosses) distribution of the orbit aspect ratio for a shell of satellites on eccentric orbits extracted from the distribution function of the galaxy (run BT1); here $N(> R_{\min}/R_{\max})$ is the number of fragments with orbit aspect ratio greater than the value given on the *x*-axis.

values of $R_{\min}/R_{\max}$ for the 20 fragments in the simulation. The quantity $N(>R_{\min}/R_{\max})$ on the *y*-axis is the number of fragments with ratio $R_{\min}/R_{\max}$ greater than the value shown on the *x*-axis. The simulation was stopped at time $t_{\text{fin}} = 120t_{\text{d}}$. By comparing the initial distribution of points (filled squares) with that of the final configuration (crosses), we can conclude that the number of fragments with eccentric orbits actually *increases* during the simulation.

4.2.3. Role of the density concentration and of the pressure anisotropy of the galaxy

The study of additional models with different density profiles and different amounts of pressure anisotropy basically confirms the general trends noted so far.
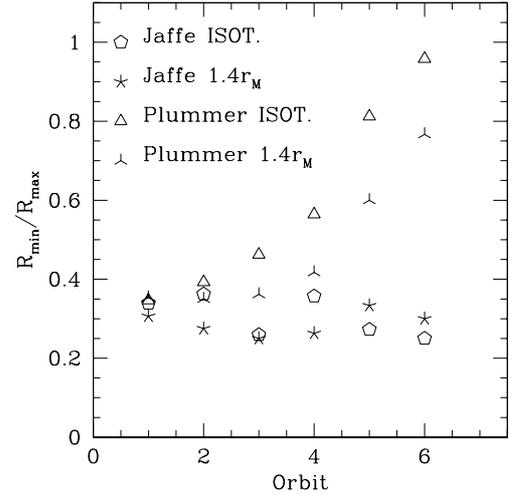
For single satellites initially placed on quasi-circular orbits, the fall time in radially anisotropic models is somewhat shorter than in models with the same density distribution but with isotropic pressure. In particular, the fall time in the most anisotropic Plummer model ($r_\alpha = 1.4r_M$; more anisotropic models are unstable) is 92% of that in the isotropic model; in the most anisotropic Jaffe model ($r_\alpha = 0.75r_M$) it is 78% of that in the corresponding isotropic model. The fall time in less concentrated models is slightly longer than in more concentrated models.

In broad core models (polytrope and Plummer), initially eccentric orbits are almost fully circularized by dynamical friction, independently of the amount of pressure anisotropy present; instead, in concentrated models (Jaffe) circularization does not take place (see Fig. 10), as observed in $f^{(v)}$ models.

We may expect that the orbit of a satellite will be circularized if the rate of loss of angular momentum is negligible with respect to the rate of loss of energy; in the opposite situation, the orbit is expected to become more eccentric. As to the relative loss rates, in the simulations we have observed a rather complex behavior, as represented in the E_s–J_s plane. Here $E_s = E_{\text{sat}}/M_s$ is the satellite specific energy and J_s is its specific angular momentum. Relating diagrams of this type to some simple theoretical expectations (based on the structure of orbits for the unperturbed spherical potential associated with the galaxy) is difficult, because in the simulations the satellite has finite mass and the galaxy is evolving. Figure 11 thus compares the orbits of two runs for a single satellite falling in a broad core model (Plummer; left frame) or in a concentrated model ($f^{(v)}$ with $\Psi = 5$; right frame). In each galaxy model, the two runs represent a case of an initial quasi-circular orbit ($v_{0s}/v_c \approx 1$; dotted line) and a case of an initially eccentric orbit ($v_{0s}/v_c = 0.5$; solid line). The orbits in the E_s–J_s plane are followed by the satellite moving from the upper right to the lower left part of the plane. The effect of circularization in one case and of lack of circularization in the other case are thus demonstrated.
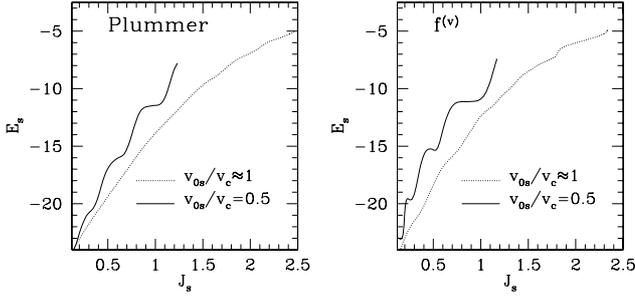
Fig. 11. Orbits in the specific energy – specific angular momentum plane. The decay of an initially quasi circular orbit ($v_{0s}/v_c \approx 1$; dotten line) is compared to that of an initially eccentric orbit ($v_{0s}/v_c = 0.5$; solid line), for a broad core galaxy model (*left frame*) and for a concentrated model (*right frame*). Along each curve, the satellite moves from the upper right to the lower left of the plane. The specific satellite energy $E_s = E_{sat}/M_s$ and angular momentum J_s are given in code units.

5. The evolution of the host galaxy induced by dynamical friction

As a result of the interactions that determine dynamical friction on a satellite or on a shell of fragments, the galaxy slowly evolves.

The models of the $f^{(\nu)}$ family that we have considered range from systems with relatively high Ψ, with projected density profiles well fitted by the $R^{1/4}$ law characteristic of the luminosity profiles of elliptical galaxies, to systems with $\Psi = 4$. For smaller values of Ψ the models would be unstable with respect to the radial orbit instability (Polyachenko & Shukhman 1981; Trenti & Bertin 2005). One reason why we have decided to study the problem of dynamical friction for models close to the margin of the radial orbit instability is that we would like to test whether, under such conditions, the response of the galaxy to the presence of infalling satellites may be significantly enhanced by internal collective effects.

We have found that a single satellite and a shell of fragments induce significantly different forms of evolution in the host galaxy. In addition, we have found the unexpected result that a single satellite, under appropriate conditions, can significantly alter the state also of firmly stable systems. In all this, we should keep in mind that in the simulations of the fall of a single satellite, in general we are considering a rather heavy satellite ($M_s = 0.1M$); clearly, lighter satellites are expected to produce less prominent effects.

5.1. Evolution induced by the fall of a single satellite on firmly stable systems

The effects of the fall of a single satellite on the density profile of the host galaxy are approximately independent of the eccentricity of its orbit (an example is given in Fig. 12, where the dashed line refers to a quasi-circular orbit and the solid line to a highly eccentric orbit). The evolution of the density profile of the host galaxy is in the direction of a softening of the initial density concentration (see also discussion in Paper II).

On the other hand, within the firmly stable part ($\Psi > 4$) of the sequence of $f^{(\nu)}$ models, the final state attained by the galaxy in the case of the capture of a single satellite does depend significantly on the initial eccentricity, as measured by v_{0s}/v_c, of the satellite orbit. In fact, in contrast with the quasi-independence of the final density profile from the eccentricity of the orbit of the satellite, the effects on the pressure anisotropy profile are sizable
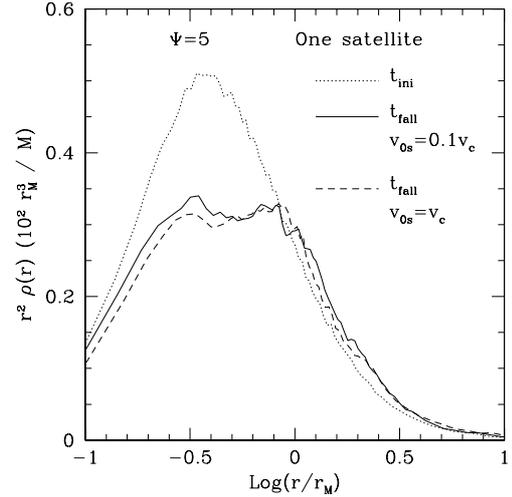

Fig. 12. Evolution of the density profile of the host galaxy induced by the fall of a single satellite. The initial galaxy density profile, multiplied by the volume factor so as to better illustrate the mass distribution, is given by the dotted line. The final density profiles of the galaxy, after the fall of a single satellite on a circular (dashed line, run $F18$) and on a highly eccentric (solid line, run $F31$) orbit, are similar.
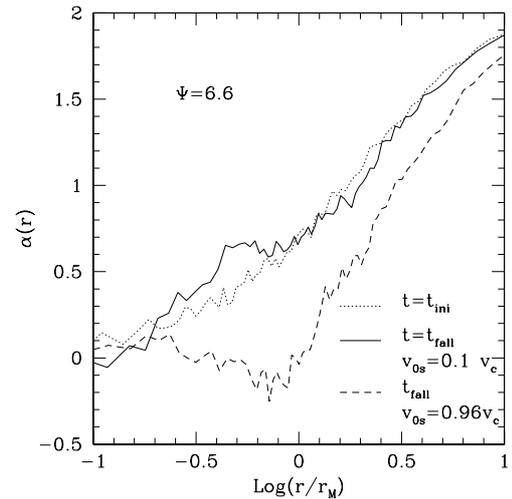

Fig. 13. Evolution of the pressure anisotropy profile induced on the $f^{(\nu)}$ model with $\Psi = 6.6$ by the fall of a single satellite on orbits characterized by different eccentricities. The initial pressure anisotropy profile is given by the dotted line. The solid line represents the final profile for a capture on a highly eccentric orbit (run $F32$); the dashed line shows the final profile for a fall on a quasi-circular orbit (run $F17$). In the latter case, note the development of an inner highly isotropic core surrounded by a tangentially biased shell, inside the external radially anisotropic envelope.

(see the example given in Fig. 13), and so are those on the final shape of the galaxy.

Therefore, we have identified two different types of behavior that split the $\Psi - v_{0s}/v_c$ plane in two regions separated by a transition boundary. In the first region (that we will call region of "negative feedback" evolution), the galaxy evolves slowly only due to dynamical friction, while in the second region (that we will call region of "positive feedback" evolution) evolution appears to be governed by the combined effect of dynamical friction and of the radial orbit instability. A schematic description of the available regimes is given in Fig. 14.
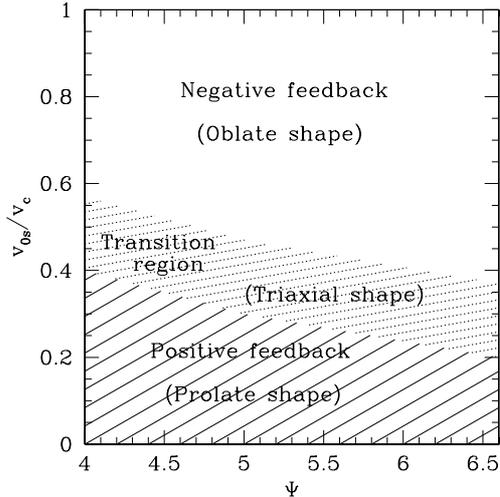
Fig. 14. Different regimes of evolution induced by the fall of a single satellite in $f^{(v)}$ galaxy models. The diagram refers to a satellite of radial size $R_s = 0.33 r_M$ and mass $M_s = 0.1M$. In the upper region ("negative feedback") the galaxy evolves slowly towards an oblate configuration. In the lower region ("positive feedback") the galaxy changes its shape significantly into a prolate spheroid. In the transition region the galaxy reaches a generic triaxial shape.

5.1.1. The "negative feedback" region

The evolution of the galaxy in the negative feedback region is illustrated in the right column of Fig. 15, which uses the examples offered by the behavior of the $f^{(v)}$ model with $\Psi = 5$.

The capture of a satellite on a quasi-circular orbit leads to final configurations characterized by a central isotropic core surrounded by a radially anisotropic envelope (see top right panel of the figure). The global anisotropy parameter k decreases towards a final value smaller than the initial one. The final configuration of the galaxy is characterized by rotation that in the inner parts (out to $\approx r_M$) is rigid (as observed in the polytropic model; see Paper I), and in the outer parts is differential and tends to disappear (see bottom right panel). During evolution, the shape of the galaxy changes into an oblate configuration (middle right panel).

Note that the net effect of the satellite is to "sweep away" the radial anisotropy present, and thus goes in the direction of removing a possible source of radial orbit instability. The final shape generated basically reflects the transfer of angular momentum from the satellite to the galaxy.

5.1.2. The "positive feedback" region

In this region the satellite is captured on highly eccentric or quasi-radial orbits (see left column of Fig. 15).

The final pressure anisotropy profile differs substantially from that attained in the negative feedack regime. The pressure anisotropy profile remains basically unchanged, with a slight increase of radial anisotropy in the central region (top left panel). Indeed, the global anisotropy parameter k increases. The trend is thus in the direction of making the radial orbit instability active. The final shape is that of a prolate spheroid (middle left panel) and this can be seen as a combined effect of the transfer of energy and momentum from the satellite to the galaxy and the possible excitation of the radial orbit instability. Little or no rotation is noted in the final configuration (bottom left panel).

5.1.3. The transition region

In this region the heavy object moves on intermediate eccentricity orbits. The qualitative behavior of the final density profile is similar to that found for other conditions (see Fig. 12). The pressure anisotropy profile remains basically unchanged (top central panel of Fig. 15; the global anisotropy parameter remains constant). The system reaches a final configuration with a generic triaxial shape (middle central panel) and little or no rotation (bottom panel).

5.1.4. Varying Ψ

Higher Ψ models are more isotropic and more concentrated and tend to be changed less in the course of the evolution from their initial state induced by the interactions with a satellite.

A curious behavior occurs in high-Ψ models. As we noted, a single falling satellite on a quasi-circular orbit, tends to change the pressure anisotropy in the tangential direction. On such high-Ψ models, which have only small amounts of pressure anisotropy in the radial direction, the effect of a satellite is such that evolution can lead to a configuration characterized by the presence of a *tangentially* biased anisotropic shell positioned between the inner isotropic core and the external radially anisotropic envelope (see Fig. 13).

In the negative feedback regime, the flattening of the oblate shape induced in the galaxy becomes smaller as one moves to models that are characterized by higher values of Ψ; correspondingly, in the positive feedback regime the prolate spheroid that is generated becomes less elongated (see Fig. 16). In other words, models away from the margin of the radial orbit instability are generally "harder", i.e. more resistant to changes, while models closer to $\Psi = 4$ are "softer", i.e. more vulnerable.

5.1.5. Role of the density concentration and of the pressure anisotropy of the galaxy

Independently of the presence of pressure anisotropy, the evolution of the density profile induced by a satellite on a quasi-circular orbit is qualitatively similar for all models considered in this paper (polytrope, Plummer, Jaffe, and $f^{(v)}$); quantitatively, models with increasing density concentration are affected less. For a given initial density profile, the final density profile of more anisotropic models is slightly shallower (runs $PL1$, $PL3$, $PL7$, $JA1$, $JA3$, $JA5$, $JA7$).

When a satellite is dragged in on a quasi-circular orbit, all models reach a final oblate shape. For a given initial density profile, the oblate product is flatter if the model is more anisotropic to begin with.

These results can be summarized by stating that more concentrated and more isotropic stellar systems are affected less by evolution induced by dynamical friction. These results confirm the behavior showed by $f^{(v)}$ models.

5.2. Evolution induced by a spherical shell of fragments on firmly stable systems

The fall of a spherical shell (with fragments on circular or on eccentric orbits) induces a slow evolution in the density and in the pressure anisotropy profiles of the galaxy similar to that observed in the negative feedback region of the $\Psi - v_{0s}/v_c$ plane in the case of the fall of a single satellite. However, at variance with that case, the final configuration remains quasi-spherical, non-rotating, and characterized by a smoother anisotropy
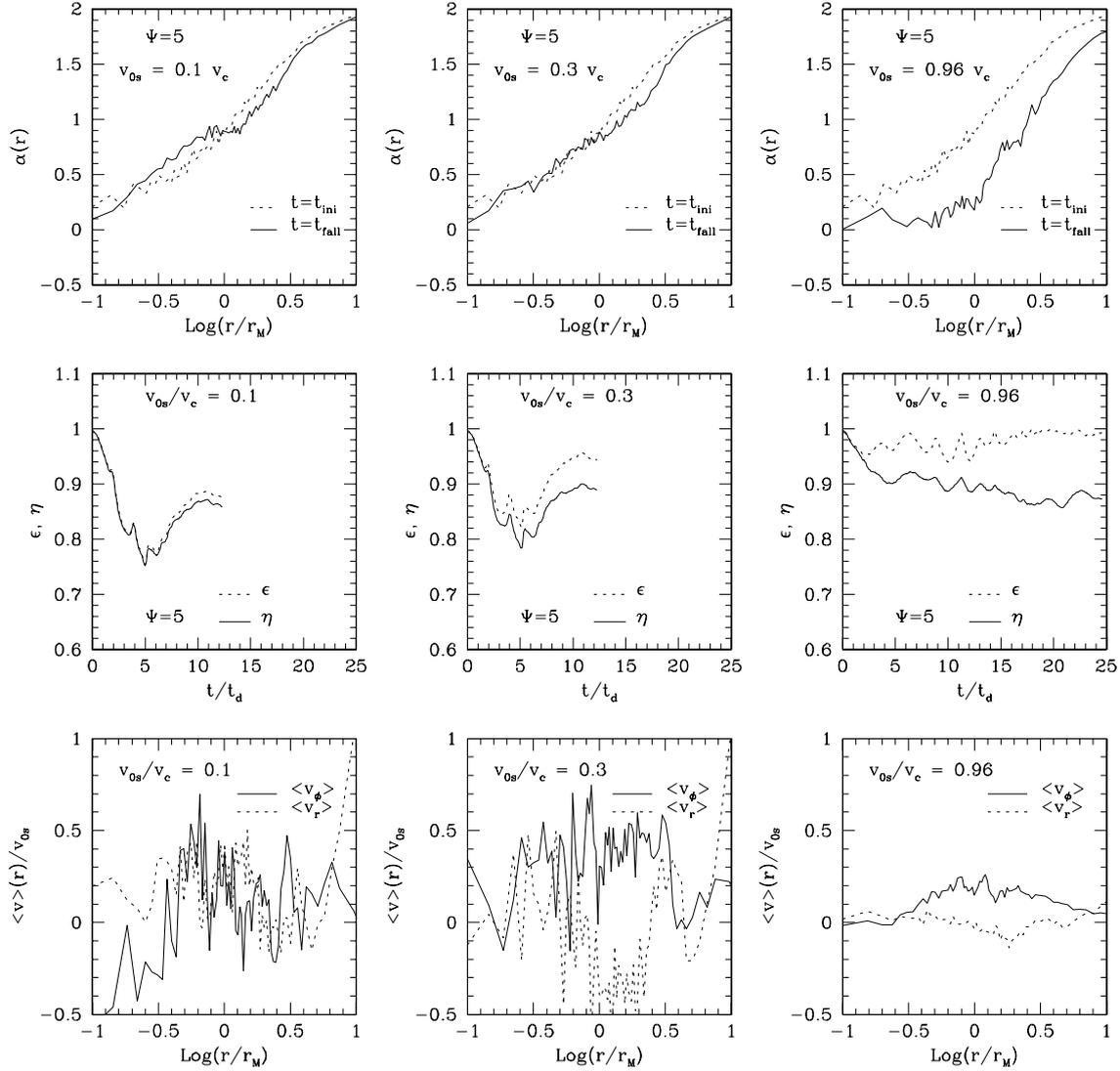
Fig. 15. Evolution induced by a single satellite in the various regimes identified in the $\Psi - v_{0s}/v_c$ plane. The left column (run $F31$) illustrates evolution in the region of positive feedback. In this regime, the pressure anisotropy profile is kept almost unchanged (*top panel*), while the galaxy evolves into a prolate spheroid (*middle panel*); some systematic motions in the radial and azimuthal directions are detected in the final quasi-equilibrium configuration, but covered by noise (*bottom panel*). The central column describes the evolution in the transition regime (run $F28$), in which the galaxy reaches a generic triaxial shape. The right column (run $F2$) describes evolution in the region of negative feedback; in this regime, the the galaxy develops a quasi-isotropic central core, an oblate shape, and significant systematic rotation in the azimuthal direction. This figure illustrates a cut of Fig. 14 at $\Psi = 5$.

profile. One example of evolution of the anisotropy profile for the $f^{(v)}$ model with $\Psi = 5$ is given in Fig. 17.

5.3. Evolution for models at the margin of the radial orbit instability

The $f^{(v)}$ model with $\Psi = 4.0$ is at the boundary between stable and unstable models (with respect to the radial orbit instability). Its evolution, as a result of interactions with a satellite or a shell of satellites, basically follows the same trends noted for firmly stable models in the previous section, with no evidence of sudden or discontinuous response.

In particular, the fall of a single satellite on a quasi-circular or lowly eccentric orbit can "sweep away" the radial anisotropy present in the central regions and thus stabilize the galaxy against the radial orbit instability. Correspondingly, the total amount of anisotropy k decreases and the shape of the galaxy

becomes oblate, with some systematic rotation. The pressure anisotropy profile becomes characterized by the particular shape visible in Fig. 18 where there is a sharp transition, at about the half-mass radius, between the central isotropic core and the external radial envelope. This shape recalls that found in some equilibria studied by Trenti & Bertin (2006), which is associated with models with global content of anisotropy k above the usually accepted threshold (Polyachenko & Shukhman 1981) for the onset of the radial orbit instability.

Instead, satellites on highly eccentric and quasi-radial orbits bring the galaxy into conditions of instability (see filled circles in Fig. 16 for $v_{0s}/v_c \approx 0.1$). The value of k is almost unchanged (top panel), but the content of radial anisotropy in the inner region increases and the shape of the galaxy becomes prolate (bottom panel).

In contrast, during the fall of a quasi-spherical shell of satellites, the galaxy maintains its round shape and absence of
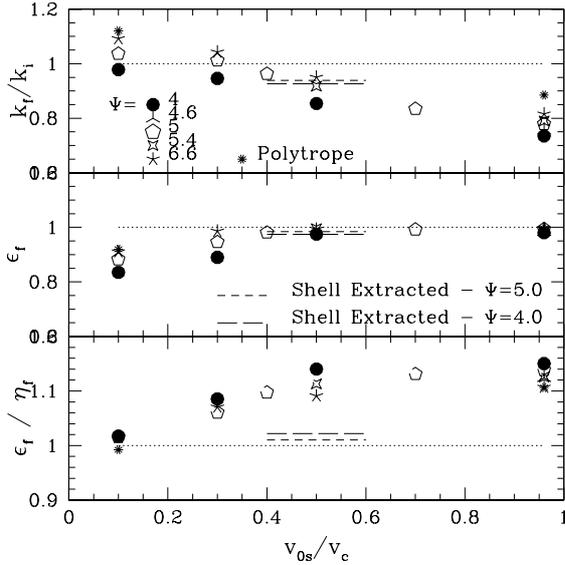
Fig. 16. Final configurations induced in some $f^{(v)}$ galaxy models by a satellite falling on orbits of different eccentricity. The *top panel* displays the ratio between the final and the initial global anisotropy parameter defined in Sect. 3.2, the *middle panel* the final value of ϵ ($\epsilon = 1$ corresponds to an oblate shape), and the *bottom panel* the ratio between the final values of ϵ and η ($\epsilon/\eta = 1$ corresponds to a prolate shape). Points on the left part of each panel are in the positive feedback region, those on the right are in the negative feedback region. Dashed and long-dashed lines refer to the final configuration induced by a spherical shell of eccentric satellites on the $\Psi = 5.0$ (run $BT1$) and $\Psi = 4.0$ (run $BT2$) models respectively.

rotation, while evolving to a less concentrated and more isotropic configuration, as for more stable $f^{(v)}$ models (long-dashed line in Fig. 16).

6. Discussion and conclusions

In this paper, by means of N-body simulations, we have addressed the problem of dynamical friction in a realistic environment (the $f^{(v)}$ models), i.e., in galaxy models characterized by significant density gradients and significant anisotropy in the velocity distribution. To understand the relative role of the two factors, density concentration and pressure anisotropy, independently of each other, we have also studied additional models with tunable (Osipkov-Merritt) pressure anisotropy profiles, for the cases of a Plummer and of a Jaffe density distribution. The properties of dynamical friction have been analyzed in terms of the effects on the orbit of a satellite (or a shell of fragments) and of the corresponding evolution induced in the stellar system.

We have found that the density concentration of the host galaxy has a significant impact on the strength of dynamical friction, while the presence of pressure anisotropy appears to be less important. In broad core models, the process of dynamical friction can be described by the classical theory of Chandrasekhar, at least approximately, with a smaller value of the Coulomb logarithm. In contrast, concentrated models, better suited to describe the density distribution of some real elliptical galaxies, are difficult to reconcile with the classical theory, because the effective value of the Coulomb logarithm would formally change with radius. Fortunately, this behavior appears to be reasonably well reproduced by the use of a simple modification of the classical Coulomb logarithm, proposed by Just & Peñarrubia (2005). In this respect, and in view of current discussions of cusp
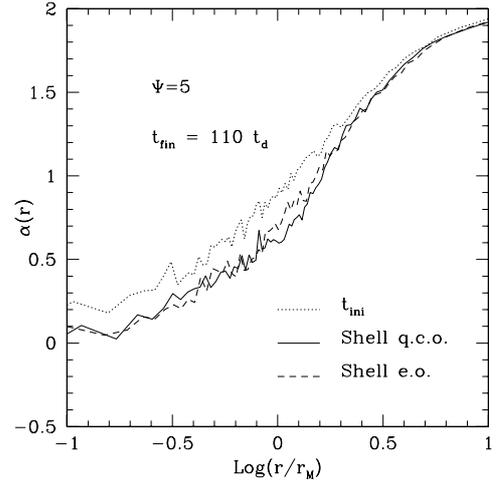

Fig. 17. Evolution of the pressure anisotropy profile induced on the galaxy by the fall of a spherical shell of fragments. The solid line refers to evolution induced by a shell of fragments on quasi-circular orbits (run $B1$) while the dashed line to evolution by a shell of fragments on eccentric orbits (run $BT1$). The final profiles are very similar in the two cases.
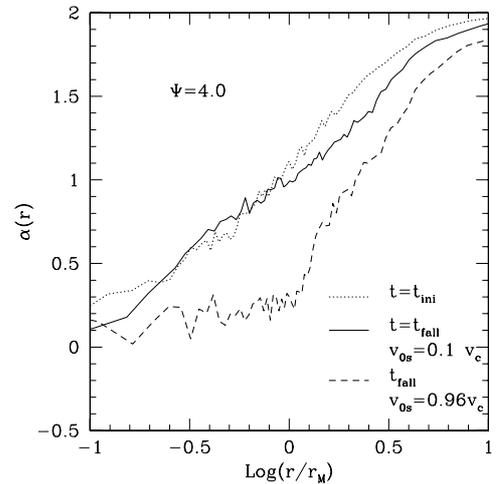

Fig. 18. Evolution of the pressure anisotropy profile induced on the most radially anisotropic model simulated ($\Psi = 4.0$). Fall on a quasi-radial orbit (run $F30$) leads to some increase of the pressure anisotropy in the radial direction inside the half-mass radius and a corresponding decrease in the external region. Fall on a circular orbit (run $F14$), instead, leads to the formation of a quasi-isotropic core of radius just smaller than r_M, surrounded by a radially anisotropic envelope.

formation and evolution in self-gravitating systems, it should be noted that the variation of the empirical Coulomb logarithm in the innermost regions ($M(r)/M < 0.2$) turns out to be rather modest, even for concentrated systems. In addition, while in broad-core models, dynamical friction tends to circularize the orbit of captured satellites, in concentrated models it does not. One curious finding, irrespective of the density concentration of the host galaxy, is that apparently the dynamical friction felt by satellites falling on eccentric orbits is stronger for inbound than for outbound satellites.

As to the evolution induced in the galaxy by the fall of heavy objects by dynamical friction, we have found the following results. Dynamical friction leads to a decrease in the central density of the host galaxy. The fall of a single satellite makes a galaxy evolve into different final shapes and phase spaceproperties. In particular, a satellite on a quasi-radial orbit induces

evolution towards a prolate shape and to more (radially) anisotropic configurations, while a satellite on a quasi-circular orbit leads to an oblate shape with pressure anisotropy changed in the tangential direction and with some rotation. The induced softening in the density distribution and the changes in the pressure anisotropy are stronger in the case of a single satellite and for less concentrated and more radially anisotropic systems; they are less pronounced in more concentrated and more isotropic models.

The experiments performed in this paper show that the shape of an otherwise collisionless stellar system can be significantly modified by the capture of a single satellite of finite but relatively small mass, with the final configuration being oblate, prolate or even triaxial, depending on the orbital characteristics of the encounter. Therefore, we argue that this process (which, in certain regimes, may couple to the stability properties of the galaxy with respect to the radial orbit instability) should be considered as one important cause for the distribution of shapes among elliptical galaxies, while, traditionally, such distribution was ascribed to the role of instabilities in more abstract terms, especially in terms of processes taking place during formation via collisionless collapse (e.g., see Aguilar & Merritt 1990; Cannizzo & Hollister 1992; Theis & Spurzem 1999; Warren et al. 1992). We have checked that the softening of the central density profile, induced by dynamical friction, does not affect substantially the projected density profile of the host stellar system that remains well described by the $R^{1/4}$ law; this agreement is better in more concentrated models, because they are originally closer to the $R^{1/4}$ law. In other words, this study of dynamical friction may have led to identifying one other important role of minor mergers in determining the evolution of galaxies into their currently observed morphologies.

References

Arena, S. E., Bertin, G., Liseikina, T., & Pegoraro, F. 2006, A&A, 453, 9 (Paper II)
Aguilar, L., & Merritt, D. 1990, ApJ, 354, 33
Bertin, G., & Trenti, M. 2003, ApJ, 584, 729
Bertin, G., Liseikina, T., & Pegoraro, F. 2003, A&A, 405, 73 (Paper I)
Binney, J. 1977, MNRAS, 181, 735
Binney, J., & Tremaine, S. 1987 (Princeton, New Jersey: Princeton University Press)
Bontekoe, Tj. R. 1988, Ph.D. Thesis, Groningen University, Groningen (B88)
Bontekoe, Tj. R., & van Albada, T. S. 1987, MNRAS, 224, 349 (BvA87)
Cannizzo, J. K., & Hollister, T. C. 1992, ApJ, 400, 58
Chandrasekhar, S. 1943, ApJ, 97, 255
El-Zant, A., Shlosman, I., & Hoffman, Y. 2001, ApJ, 560, 636
El-Zant, A., Hoffman, Y., Primack, J., Combes, F., & Shlosman, I. 2004, ApJ, 607, L75
Evans, N. W., & Collett, J. L. 1997, ApJ, 480, L103
Fujii, M., Funato, Y., & Makino, J. 2005, PASJ, 58, 743
Ghigna, S., Moore, B., Governato, F., et al. 2000, ApJ, 544, 616
Hashimoto, Y., Funato, Y., & Makino, J. 2003, ApJ, 582, 196
Jaffe, W. 1983, MNRAS, 202, 995
Jiang, I. G., & Binney, J. 2000, MNRAS, 314, 468
Just, A., & Peñarrubia, J. 2005, A&A, 431, 861
Kandrup, H. E. 1983, Ap&SS, 97, 435
Ma, C.-P., & Bertschinger, E. 2004, ApJ, 612, 28
Ma, C.-P., & Boylan-Kolchin, M. 2004, Phys. Rev. Lett., 93, 021301
Merritt, D. 1985, AJ, 90,1027
Mulder, W. A. 1983, A&A, 117, 9
Moore, B., Governato, F., Quinn, T., Stadel, J., & Lake, G. 1998, ApJ, 499, L5
Navarro, J. F., Frenk, C. S., & White, S. D. M. 1996, ApJ, 462, 563
Navarro, J. F., Hayashi, E., Power, C., et al. 2004, MNRAS, 349, 1039
Nelson, R. W., & Tremaine, S. 1999, MNRAS, 306, 1
Nipoti, C., Treu, T., Ciotti, L., & Stiavelli, M. 2004, MNRAS, 355, 1119
Osipkov, L. P. 1979, SvAL, 5, 42
Palmer, P. L., & Papaloizou, J. 1985, MNRAS, 215, 691
Peñarrubia, J., Just, A., & Kroupa, P. 2004, MNRAS, 349, 747
Polyachenko, V., & Shukhman, I. 1981, Soviet Astron., 25, 533
Spinnato, P. F., Fellhauer, M., & Portegies Zwart, S. F. 2003, MNRAS, 344, 22
Stiavelli, M., & Bertin, G. 1987, MNRAS, 229, 61
Theis, C., & Spurzem, R. 1999, A&A, 341, 361
Tremaine, S., Ostriker, J. P., & Spitzer, L. 1975, ApJ, 196, 407
Tremaine, S., & Weinberg, M. D. 1984, MNRAS, 209, 729
Trenti, M. 2005, Ph.D. Thesis, Scuola Normale Superiore, Pisa
Trenti, M., & Bertin, G. 2005, A&A, 429, 161
Trenti, M., & Bertin, G. 2006, ApJ, 637, 717
Trenti, M., Bertin, G., & van Albada, T. S. 2005, A&A, 433, 57
van den Bosch, F. C., Lewis, G. F., Lake, G., & Stadel, J. 1999, ApJ, 515, 50
Warren, M. S., Quinn, P. J., Salmon, J. Z., & Zurek, W. H. 1992, ApJ, 399, 405
Weinberg, M. D. 1986, ApJ, 300, 93
Weinberg, M. D. 1989, MNRAS, 239, 549
Weinberg, M. D. 2001, MNRAS, 328, 321
White, S. D. M. 1976, MNRAS, 174, 467